First-principles calculation of Mg/MgO interfacial free energies

Wenwu Xu[1,2], Andrew P. Horsfield[3*], David Wearing[3], and Peter D. Lee[1,2†]
[1]*Manchester X-ray Imaging Facility, University of Manchester, Manchester M13 9PL, UK,*
[2]*Research Complex at Harwell, Didcot OX11 0FA, UK*
[3]*Department of Materials, Imperial College London, South Kensington Campus, London SW7 2AZ, UK*

[*]a.horsfield@imperial.ac.uk; Tel(Fax): +44 20 7594 6753(7)
[†]peter.lee@manchester.ac.uk; Tel: +44 12 3556 7789

ABSTRACT

Interfacial free energies strongly influence many materials properties, especially for nanomaterials that have very large interfacial areas per unit volume. Quantitative evaluation of interfacial free energy by means of computer simulation remains difficult in these cases, especially at finite temperature. Density Functional Theory (DFT) simulation offers a robust way to compute both the energies and structures of the relevant surfaces and interfaces at the atomic level at zero Kelvin, and can be extended to finite temperatures in solids by means of the harmonic approximation (HA). Here we study the Mg/MgO interface, employing DFT calculations within the HA to obtain its key physical properties. We calculate the free energies of several key surfaces/interfaces when the temperature (T) increases from 0 K to 800 K, finding that all free energies decrease almost linearly with T. We have considered two surfaces, Mg(0001) (0.520 to 0.486 J/m^2), and MgO(100) (0.86 to 0.52 J/m^2), and two Mg(0001)//MgO(100) interfaces with the Mg-Mg and Mg-O stacking sequences at the interface planes (1.048 to 0.873 J/m^2 and 0.910 to 0.743 J/m^2 respectively). Using these values we determine the interfacial free energy as a function of temperature and size for MgO nanoparticles in solid Mg, an important metal matrix nanocomposite material.

Keywords: interfacial free energy; density functional theory; metal matrix nanocomposite; Mg/MgO interface.

1. Introduction

When the size of a material in at least one dimension is at the nanometer scale, the corresponding interfacial properties cannot be easily interpreted based on simple atomic or solid solution theories [1]. While significant effort has been made to understand the observed phenomena, even with the most advanced techniques for studying interfaces many observations remain to be fully explained [1]. A necessary first step is to formulate a quantitative method to compute the energy associated with interfaces; this will help us understand properties which are relevant to many areas of physics, chemistry, engineering, and other disciplines [2, 3].

In the research field of structural materials, current eco-energy challenges, particularly in the aerospace and auto sectors, can only be met by a new generation of light metals that take us beyond the contemporary strength to weight limits [4, 5]. Embedding nanoparticles (NPs) into existing metallic alloys (termed metal matrix nanocomposites, or MMNCs) can yield a step change in mechanical properties [6-8]. However, to achieve the desired mechanical properties, reinforcing NPs must be distributed uniformly within the metallic matrix of the composite [9-11]; because NPs tend to agglomerate during metallurgy processing due to their low wettability, this is difficult to achieve. It is the interfacial energy between the NPs and the metal that governs the wettability, making this a key parameter.

Despite the importance of interfacial energies for determining the MMNC properties, they are difficult to determine accurately by experiment, and hence quantitative analysis has rarely been performed and a full understanding has not been obtained. Computer simulation is an important alternative method to investigate interfacial properties. With the sustained exponential growth in computer resources, the impact of simulation can only increase [12].

Various modelling methodologies at multiple scales such as density functional theory (DFT) [13, 14], molecular dynamics (MD) [15, 16], phase field (PF) modelling [17, 18] and Monte Carlo (MC) methods [19, 20] have been developed to calculate the interfacial energy

in condensed matters systems. The combination of DFT and MD is especially appealing as it allows us to retain an accurate description of the cohesion while including the nuclear dynamics associated with finite temperatures [21, 22]. However, it is a computationally expensive approach and for many cases less costly alternatives are necessary.

In this work, we focus on the calculation of the interfacial free energy of heterophase interfaces in MMNCs using DFT within a harmonic approximation (HA) for the nuclear motion. This approximation is reliable at low temperatures when the amplitude of oscillation of the nuclei is small. It becomes less accurate as temperature increases, though it is expected to give the right trends. Thermodynamic Integration (TI) using constant pressure molecular dynamics could provide more accurate results at higher temperature, but is vastly more expensive; the use of TI to compute interfacial energies will be investigated in future work. As a representative example of the interfaces found in MMNCs, we consider one often found in Mg-based alloys, namely Mg/MgO. A quantitative understanding of its structure and interfacial free energy at the atomic level is important for the design and development of relevant nanocomposite alloys. In addition, Mg/MgO interfaces can also play an important role in several other applications such as interfacial superconductivity [23, 24] and tunnelling spin polarization [25, 26].

2. Method

We model the interface A-B as an atomically sharp junction between bulk phases A and B. Interfacial defects such as steps and roughness are not considered in this work which usually requires large interface unit cells containing thousands of atoms, resulting in our DFT simulations becoming too expensive. Even though HRTEM measurements [27] show that interfaces are not atomically flat over large distances, over the distances spanned by our computational cells, this is a valid approximation. The interfacial free energy $\gamma(T)$ can be obtained as a function of temperature using a slab technique [28]. As shown in Fig. 1, there

are at least two approaches [28-30]: the first is to have alternating slabs of A and B (which are cleaved from bulk phases A and B along certain orientations) with identical atomic structures at the interface planes (Fig. 1a); in the second an interface slab containing one interface and two surface planes is separated from its periodic images by vacuum (Fig. 1b). In both types of models, the distance between neighbouring interface or surface planes should be large enough to avoid interactions so that the bulk features of components between interface planes are described properly.

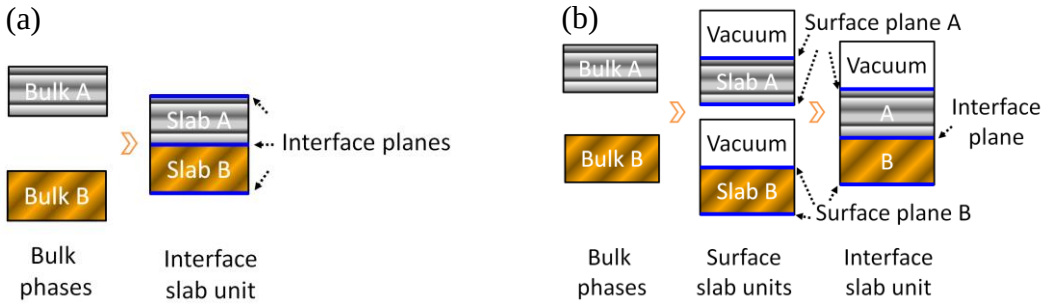

Fig. 1. Two approaches for constructing the interface model using slab techniques: (a) alternating slabs of A and B cleaved from bulk phases along certain crystallographic orientations; (b) surface/interface units are separated from their periodic images by vacuum. Surface and interface cell units repeat in the directions normal to the surface/interface planes.

Each approach has both advantages and disadvantages. The first contains only one type of interface, so its energy can be readily computed by subtracting the energies of bulk phases of A and B from the energy of the slab. However, it requires the cell to be relaxed along the direction perpendicular to the interface (to remove artificial stresses at the interface), and can only be applied when both interfaces in the cell are identical. The second approach naturally allows for stress relief at the interface when the atoms relax, and can be applied to more general types of interface. However, there is extra computational expense associated with determining the energies of the exposed surfaces, as well as the slab and bulk calculations.

It should be noted that bulk phases are usually strained in order to match at the interface as they generally have different lattice parameters. Consequently, if we define the interfacial energy to be the difference in energy between the slab and the corresponding amounts of relaxed bulk material (see Fig. 2a), then the interfacial free energies include a contribution from stress due to the lattice mismatch between the two sides of interface. This is not a useful definition as the interfacial energy now depends on how many strained layers of the bulk are retained in the calculation. The interfacial energy thus needs to be defined relative to the strained bulks (see Fig. 2b).

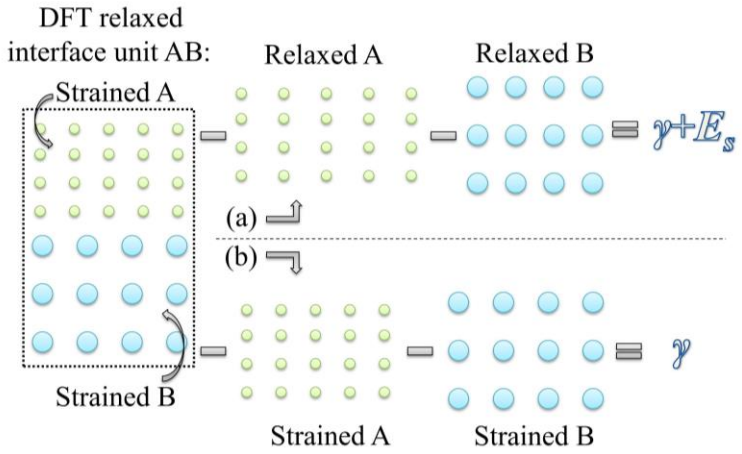

Fig. 2. Computing interfacial free energy based on DFT: (a) by subtracting off total energies of relaxed A and B from that of the relaxed interface unit, the result includes interfacial free energy (γ) and the strain energy (E_s); (b) by subtracting off total energies of strained A and B from that of relaxed interface unit, the result includes only the interfacial free energy (γ).

In the following we describe a method for computing the interfacial free energy and the strain energy associated with the lattice mismatch at the interface planes using the aforementioned first approach (see Fig. 1a) because of its lower computational cost in this case. We build our computational interface slab cell so that we have identical atomic

structure at the two interfaces between alternating slabs. The interfacial free energies γ can then be computed using:

$$\gamma(T) = \frac{1}{2S_{int}}\left[F_{slab}^{AB}(T) - \sum_{i\in\{A,B\}} F_S^{(i)}(T)\right] \quad (1)$$

where S_{int} denotes the area of an interface and the factor 2 is to account for the fact that there are two identical interfaces per computational cell. F_{slab}^{AB} is the Helmholtz free energy of the interface slab and $F_S^{(i)}$ is the free energy of the strained supercell of phase *i* (A or B) which consists of the same atomic numbers and in plane lattice parameters as that in the corresponding interface models, but allowing the z-direction (*c* lattice direction) of the supercell to relax.

To quantify the strain contributions when calculating the interfacial free energies, we subtract off the strain free energy E_s by taking the total energy difference between the distorted supercells which have the lattice parameters taken from the corresponding interface model, and the fully relaxed bulk phases. However, we should bear in mind that in reality dislocations may form to relieve the strain once a layer is thick enough that the strain energy exceeds the dislocation formation energy [31]. We calculate E_s via:

$$E_S(T) = \sum_{i\in\{A,B\}}(F_S^{(i)}(T) - N_i F_{bulk}^{(i)}(T)) \quad (2)$$

where $F_{bulk}^{(i)}$ is the free energy per formula unit of the relaxed bulk phase *i* and the interface slab contains N_i formula units of component phase *i*.

In Eqs. (1) & (2), the Helmholtz free energy *F* at temperature *T* and volume *V* of crystalline solids can be written as the sum of the internal energy U_0 in the static ground state (atoms relaxed to their lowest energy configurations, without any vibrations), the vibrational free energy, F_{vib}, and the electronic excitation free energy, F_{el} [32, 33]:

$$F(V,T) = U_0(V) + F_{vib}(V,T) + F_{el}(V,T) \quad (3)$$

In the harmonic approximation the volume takes the ground state equilibrium value V_0. In Eq. (3), U_0 can be obtained from DFT calculations. Far below the melting point, F_{vib} is well described by the harmonic approximation [34]:

$$F_{vib} = k_B T \sum_{\boldsymbol{q},i} ln\left\{2 \sinh\left[\frac{\hbar\omega_{q,i)}}{k_B T}\right]\right\} \quad (4)$$

where $\omega_{\boldsymbol{q},i}$ is the frequency of the ith phonon mode with wave vector $\boldsymbol{q}$, which is evaluated at constant volume in the framework of density functional perturbation theory (DFPT) [34]. The sum in Eq. (4) is over all phonon modes and over all wave vectors in the first Brillouin zone and $\hbar$ is the reduced Plank constant. The electronic contribution to the free energy $F_{el}=E_{el}-TS_{el}$ is obtained from the electronic density of states using the standard formulae for E_{el} and S_{el} [35, 36]. The electronic excitation free energy is negligible at temperatures far below the melting point [34].

By combining the above equations, and ignoring the contribution from electronic excitations, the temperature dependence of the interfacial free energy in Eq. (1) can be expressed as:

$$\gamma(T) = \gamma_0 + \frac{1}{2S_{int}}\left[F^{AB}_{slab_{vib}}(T) - \sum_{i\in\{A,B\}} F^{(i)}_{S_{vib}}(T)\right] \quad (5)$$

where γ_0 is the interfacial energy at the ground state (0 K), neglecting the zero point motion of the nuclei. $F_{slab_{vib}}$ and $F^{(i)}_{S_{vib}}$ are the vibrational free energies of the interface slab and the strained supercell for phase i, respectively.

The strain contribution to free energy in Eq. (2) can now be written as

$$E_S(T) = \sum_{i\in\{A,B\}}\left[E^{(i)}_S(0K) + E^{(i)}_{S_{vib}}(T)\right] \quad (6a)$$

$$E_S(T) = \sum_{i\in\{A,B\}}\left[\left(U^{(i),0}_S - N_i U^{(i),0}_{bulk}\right) + \left(F^{(i)}_{S_{vib}}(T) - N_i F^{(i)}_{bulk_{vib}}(T)\right)\right] \quad (6b)$$

In Eq. (6), the first term, $E^{(i)}_S(0K) = U^{(i),0}_S - N_i U^{(i),0}_{bulk}$, represents the difference of total energies between the strained supercell and the relaxed bulk phase at the ground state, and is

the strain energy of the interface unit at 0 K. The second term, $E_{S_{vib}}^{(i)}(T) = F_{S_{vib}}^{(i)}(T) - N_i F_{bulk_{vib}}^{(i)}(T)$, describes the vibrational contribution to the strain energy and $F_{bulk_{vib}}^{(i)}$ is the vibrational free energy of the relaxed bulk phase *i*.

Combining Eqs. (5) and (6), we can describe explicitly the strain contributions of each component phase in the interface unit when calculating the interfacial free energies by Eq. (7),

$$\gamma(T) = \gamma_0 + \frac{1}{2S_{int}}\left[F_{slab_{vib}}^{AB}(T) - \sum_{i\in\{A,B\}}\left(N_i F_{bulk_{vib}}^{(i)}(T) + E_{S_{vib}}^{(i)}(T)\right)\right] \quad (7)$$

To verify the accuracy of our calculations we would like to compare our results with those from previous work. For this we compute surface energies and the work of separation, as these appear in the literature. The ground state interfacial energy is related to the ground state ideal work of separation W^0_{sep}, which in turn is defined as the reversible work needed to separate the interface into two free surfaces [37]:

$$W_{sep}^0 = \sigma_A^0 + \sigma_B^0 - \gamma_0 \quad (8)$$

The surface energies σ^0_A and σ^0_B are similarly computed from the static ground state (at 0 K). We note that the temperature dependence of a surface free energy (e.g., surface slab A in Fig. 1) can be calculated using:

$$\sigma_A(T) = [F_{slab}^{(A)}(T) - N_A F_{bulk}^{(A)}(T)]/2S_{sur} \quad (9)$$

where S_{sur} is the surface area. The surface free energy $\sigma_A(T)$ can then be expressed as:

$$\sigma_A(T) = \sigma_A^0 + \sigma_A^{vib}(T) \quad (10)$$

where σ_A^{vib} is the temperature dependent vibrational contributions to the surface energy.

3. Computational details

3.1. Geometry of the Mg/MgO interface

By oxidizing pure metal Mg, Hayden [38] and Kooi [39] et al. have identified two different crystal orientation relationships (ORs) of Mg/MgO interfaces utilizing different techniques such as low energy electron diffraction (LEED) [38] and high resolution transmission

electron microscopy (HRTEM) [39], as summarized in Table 1. DFT simulations (see Supplemental Material [40]) shows that the OR II, Mg(10-10)//MgO(110) interface possesses higher interfacial energy at the ground state (0 K) than OR I. Additionally, previous DFT simulations of Mg/MgO interfaces [41] have suggested that the ground state interfacial energy of OR I, Mg(0001)//MgO(100) is lower than that of the other low-indexed Mg/MgO interfaces, including Mg(0001)//MgO(110) and Mg(0001)//MgO(111). By combining experimental and simulation analyses, we conclude that the Mg(0001)//MgO(100) interface is the most stable, having the lowest interfacial free energy at 0 K. We therefore performed first-principles calculations at finite temperatures for the Mg(0001)//MgO(100) interface, which we model as a periodic layer structure without vacuum, as we have identical atomic arrangements at both interfaces in the computational cell at this particular orientation.

Table 1. Experimental crystal orientation relationships (ORs) of Mg/MgO interfaces.

ORs	MgO($h\ k\ l$)//Mg($h\ k\ j\ l$)		$[u\ v\ w]_{MgO}$//$[u\ v\ t\ w]_{Mg}$	
I [38, 39]	(100)	(0001)	[110]	[11-20]
II [39]	(110)	(10-10)	[001]	[0001]

An ideal interface unit cell model should preserve the lattice periodicities of both slab components and contain least number of atoms in the system while keeping the interfacial strain small enough not to change significantly the atomic arrangement of interface units. The smallest size of interface unit of Mg(0001)//MgO(100) consisting of one Mg(0001) ($\sqrt{3}\times1$) cell matching an MgO(100) (1×1) cell. This results in very large lattice mismatch (e.g. $|a_{Mg(0001)}-a_{MgO(100)}|/a_{MgO(100)}$) at the interface plane, i.e. 83.6% and 7.8% along a and b direction, respectively, according to the measured bulk lattice constants of Mg (a=b=3.209 Å; c=5.218 Å) [42] and MgO (a=b=c=4.211 Å) [43]. This is practically not stable thus not be chosen for DFT simulation. We therefore chose the second smallest size of interface supercell

which is constructed from an Mg(0001) ($\sqrt{3}\times1$) cell matching an MgO(100) (2×1) cell to represent the Mg(0001)//MgO(100) interface. This model preserves the lattice periodicities of both components and has a reasonably small lattice mismatch (a few percent) at the interface planes, i.e. the lattice mismatch at the interface planes is about 6.7% along *a* lattice direction and 7.8% along *b* lattice direction.

We consider two different atomic stacking sequences at the Mg(0001)//MgO(100) interface, namely the Mg-Mg and Mg-O stacking, where Mg atoms from Mg(0001) component sit respectively on top of Mg and O atoms from the MgO(100) component. To illustrate the atomic structure of the interface models, an Mg(0001)//MgO(100) interface unit cell consisting of 5 atomic layers of each component (Mg-Mg stacking) and the corresponding Mg(0001) and MgO(100) surface slab units are presented in Fig. 3. Unless otherwise specified, all structures in this work are fully relaxed with respect to atomic coordinates and cell vectors in the framework of DFT. According to the DFT optimized lattice parameters of bulks Mg and MgO (see Table 3), the interfacial lattice mismatches are calculated to be about 7.0% and 7.5% along *a* and *b* lattice direction, respectively, consistent with the aforementioned experimental results. We note that, in the relaxed interface units, the bond lengths of Mg-Mg and Mg-O at the interface plane are different in the two interface units with different stacking sequence. This is due to the stronger chemical bonding between Mg and O as compared with Mg and Mg. We also note that we do not include the effect of O diffusion across the interface to produce a shallower concentration gradient. To determine this gradient would require a rather different approach from the one taken here. At higher temperatures the gain in configurational entropy is expected to outweigh the enthalpic penalty, but this is not expected to be significant at the room temperature, and so is neglected here.

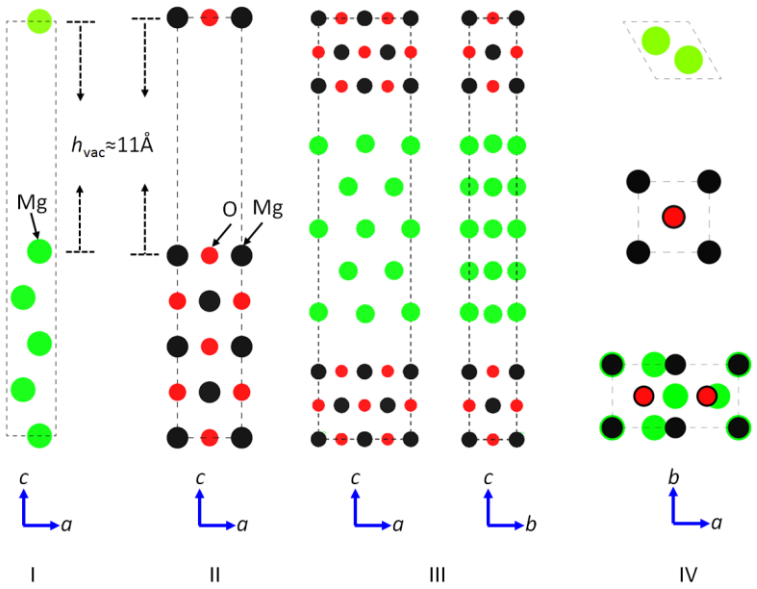

Fig. 3. (Colour online) Atomic structures of computational cells used for the DFT calculations: (I) Mg(0001) surface; (II) MgO(100) surface; (III) $Mg(0001)_{hcp}/MgO(100)_{fcc}$ interface (Mg-Mg stacking at the interface planes) viewed along an interface plane; and (IV) the corresponding top-views. *a*, *b* and *c* are the lattice parameters and the arrows show crystal orientations.

In order to accommodate the lattice mismatch at interfaces, the Mg(0001) and MgO(100) slabs should be compressed or stretched to align at the interface plane. Table 2 gives the strains (lattice distortions) of both components, i.e., Mg(0001) and MgO(100), along different lattice directions (*a* and *b*) at the interface plane for each interface model simulated from DFT. Note that the strains in Table 2 are calculated with reference to the optimized lattice parameters of Mg and MgO bulks (see Table 3) from DFT simulations computed using the same parameters (pseudopotential, planewave cutoff, *etc*) as for the interface models. It is seen that the strain behaviour at the interface plane for Mg-Mg and Mg-O stacking are different, suggesting different atomic bonding across the interface. It should be noted that the lattice mismatch in the interface plane along different directions (*i.e.*, lattice *a* and *b* directions) does not vary significantly (<0.25%) with the number of atomic

layers for both slab components provided there are more than 5 layers. The variation observed is a result of the reduction in strain energy by cell relaxation in the plane of the interface. The strain energies of both components are quantified according to the method proposed in Section II and will be discussed in detail in Section IV.

Table 2. Strains of Mg(0001) and MgO(100) slab components for the Mg(0001)//MgO(100) interface model from DFT full relaxations with respect to atomic coordinates and cell vectors.

Stacking sequence at the interface planes	Strains at the interface plane (+ stretched, - compressed)			
	along *a* direction (%)		along *b* direction (%)	
	Mg(0001)	MgO(100)	Mg(0001)	MgO(100)
Mg-Mg	+4.97	-2.36	-7.17	-0.29
Mg-O	+5.37	-1.97	-6.57	+0.36

We carried out comprehensive convergence tests for the total energies of bulk phases and free surface slabs with regard to the planewave energy cut-off and the electronic k-point sampling; energy changes are converged to less than 0.01 eV/atom. We then investigated how many layers of atoms in the interface unit are needed to avoid significant interactions between adjacent interface planes, as will be discussed in more detail in Section IV. We find that an interfacial model geometry consisting of 5 atomic layers of each component (see Fig. 3) is sufficient to compute the interfacial free energy for the Mg(0001)/MgO(100) interface to an accuracy of order of ~0.01 J/m^2. This is consistent with reported DFT calculations where a 5-layer slab of Mg(0001) was placed on 3-layers of MgO(100) to construct the interface unit cell [41]. For the surface calculations, a vacuum thickness of 10.5 Å [29] and 15-20 Å [14, 41, 44] was added respectively for MgO(001) and Mg(0001) slabs in previous calculations, while in this work we found that a vacuum gap of about 11 Å for both Mg(0001) and MgO(100)

added in the *c*-axis direction is sufficient to avoid interactions between adjacent surfaces and converge the surface energy to ~0.01 J/m^2.

3.2. Computational details

All calculations were performed using the plane wave DFT code Cambridge Serial Total Energy Package (CASTEP) [45]. The Perdew-Burke-Ernzerhof (PBE) functional [46] within the generalized gradient approximation (GGA) for the exchange and correlation energy was used. Brillouin zone integration was performed using k-points on a Monkhorst-Pack grid [47]. Norm-conserving pseudo-potentials were used with a plane-wave basis set energy cut-off of 45 Ha. The k-point mesh with spacing of 0.022 Å^{-1} in the reciprocal space was used for all the calculations including bulks, surfaces and interfaces. Self-consistent field (SCF) calculations were converged to 10^{-10} eV/atom for the total energy calculations. The geometry optimizations were run until the atomic forces were below 0.001 eV/Å. The Broyden-Fletcher-Goldfarb-Shannon (BFGS) algorithm [48] was applied to relax the atomic positions and cell vectors (unless specifically mentioned) automatically to achieve the minimum total energy of the system. These parameters converged the calculated properties to a degree measurable by experiments: 0.01 J/m^2 for surface and interfacial energies, and 0.001 Å for lattice constants.

The vibrational contribution is essential for calculating the temperature dependence of free energies of a solid crystal [49]. Phonons for bulk crystals, surfaces and interface were computed using the linear response method based on DFPT. The free energies as a function of temperature of these structures were obtained from the calculated phonon density of states utilizing standard thermodynamic expressions within the harmonic approximation (Section II). For the case of the Mg/MgO interface, we computed free energies for all relevant

structures at temperatures up to 800 K (well below the melting points of Mg (923 K) [42] and MgO (3125 K) [35]).

4. Results and discussion

4.1. Static ground state properties

The calculated lattice constants of bulk Mg and MgO, and the surface energies of Mg(0001) and MgO(100) at the static ground state are obtained from DFT simulations, as shown in Table 3. Our calculated lattice constants of bulk phases are generally consistent with experimental measurements [42, 43]. Surface energies $\sigma_{Mg(0001)}$ and $\sigma_{MgO(100)}$ under full relaxation of surface unit cells were obtained from $\sigma=(E_{slab}-nE_{bulk})/2S$ where E_{slab} is the total energy of an n-layer slab at the ground state from DFT calculations, and the value of E_{bulk} can be taken as the slope that is extracted by the straight line fitted to all of the values of total energies of the n-layer slabs versus n. S is the surface area of the unit cell. The value of $\sigma_{Mg(0001)}$ agrees well with experiment [38] and reported DFT calculations (with GGA) [41, 44] while $\sigma_{MgO(100)}$ is ~10% lower than previous results [41, 50, 51]

Table 3. Calculated physical properties at 0 K of Mg and MgO bulks, Mg(0001) and MgO(100) surfaces in comparison to experimental measurements (298 K) and reported static ground state calculations.

Structural models	This work	Experiments (298 K) or reported static ground state calculations
	Lattice constant, (Å)	
Mg	a=3.245, c=5.323; c/a=1.640	a=3.209, c=5.218; c/a=1.626 [42]
MgO	a=4.273	a=4.211 [43]
	Surface energy, σ (J/m^2)	
Mg(0001)	0.52	0.44 [38]; 0.56 [44]*; 0.63 [41]*
MgO(100)	0.86	1.15 [50]; 0.97 [41]*; 1.02 [51]*

*reported DFT calculations with GGA

The ground state interfacial energy, work of separation and the corresponding strain energy of the two models with a (√3×1)/(2×1) supercell containing an Mg(0001)/MgO(100) interface and consisting of 5 layers of each component are obtained (see Table 4). The interface with the Mg-O stacking sequence possesses a lower interfacial free energy and higher work of separation at 0 K than that of the model with Mg-Mg stacking at the interface planes. This agrees with the reported DFT simulations with GGA [41]. The difference of these values between current work and reported calculations [41] is probably mainly due to the fact that the strain contributions are included in the reported interfacial free energies. In addition, the strain energies in the two interface models are slightly different. By summing up the contributions from each component, the total strain energy of the two interface models with Mg-Mg and Mg-O stacking at the interface planes are calculated to be 0.63 eV and 0.54 eV, respectively. Note that there are 10 Mg atoms and 10 formula units of MgO atoms in the (√3×1)/(2×1) Mg(0001)/MgO(100) interface consisting of 5 layers of each component.

Table 4. Calculated interfacial energies and work of separations of the (√3×1)/(2×1) Mg(0001)/MgO(100) interface consisting of 5 atomic layers of each component, and the corresponding strain energies. Reported values are listed where relevant for comparisons.

Stacking	Interfacial energies γ_0, (J/m^2)		Work of separation W_{sep}, (J/m^2)		Strain energies, E_s (eV)	
					$E_s^{5MgO(100)}$, (eV/MgO)	$E_s^{5Mg(0001)}$, (eV/atom)
Mg-Mg	1.048	1.45*	0.332	0.14*	0.035	0.033
Mg-O	0.910	1.20*	0.470	0.39*	0.028	0.026

*reported DFT calculations with GGA in Ref. [41].

We also investigated the changes of strain energies and interfacial energies with further increase of the number of atomic layers in the interface units. For example, in the interface model with Mg-Mg stacking at the interface planes, we carried out DFT simulations for the interface models consisting of 5 atomic layers of MgO(100) and different numbers of layers of Mg(0001), and the results are shown in Table 5. The strain energy contribution from the Mg(0001) component is found to increase linearly with the increase in the number of its atomic layers and the strain energy contribution from MgO(100) component remains almost invariant. Consequently, the interfacial energies with different numbers of layers are obtained (see Table 5). As is seen, the strain-free interfacial energy at 0 K does not vary significantly when the number of atomic layers of both components is over 5. Finally, the interfacial energy and work of separation of Mg(0001)/MgO(100) with Mg-Mg stacking are then determined as 1.05±0.01 J/m^2 and 0.33±0.01 J/m^2, respectively. Similarly, the corresponding values of 0.91±0.01 J/m^2 and 0.47±0.01 J/m^2 are obtained for the interface model with Mg-O stacking at the interface planes.

Table 5. Calculated strain energies and interfacial free energies at 0 K of *n*Mg(0001)/5MgO(100) interface units with Mg-Mg stacking at the interface plane (*n*=5, 7 and 9).

n	Strain energy, E_s (eV)		Interfacial free energy, γ (J/m^2)
	$E_s^{n\mathrm{Mg(0001)}}$	$E_s^{n\mathrm{MgO(100)}}$	
5	$E_s^{5\mathrm{Mg(0001)}}$=0.352	$E_s^{5\mathrm{MgO(100)}}$=0.284	1.048
7	$E_s^{7\mathrm{Mg(0001)}}$=0.490	$E_s^{5\mathrm{MgO(100)}}$=0.281	1.056
9	$E_s^{9\mathrm{Mg(0001)}}$=0.631	$E_s^{5\mathrm{MgO(100)}}$=0.279	1.045

4.2. Temperature-dependent properties

Based on the aforementioned DFT calculations to optimize geometry, we performed phonon calculations using density functional perturbation theory (DFPT) for all the units listed in Tables II and III. The phonon spectra of Mg and MgO bulks (both contain two atoms in the primitive unit cell) have six phonon branches: one longitudinal-optical (LO), one longitudinal-acoustical (LA), two transverse-optical (TO) and two transverse-acoustical (TA) [35]. Phonon dispersions of surfaces and interfaces, defined within the two-dimensional Brillouin zone, contain as many branches as the number of atoms in the slab unit cell multiplied by three. As a consequence, the phonon spectra of surfaces and interfaces are rather complicated. The phonon calculations were performed over the entire Brillouin zone and the phonon spectra, including several high symmetry points in the first Brillouin zone, are presented here.

The calculated phonon spectrum including high symmetry points (Γ, X, W, K, L) for bulk FCC (B1) MgO is presented in Fig. 4(a). The theoretical results agree well with experimental values [52] (solid squares). For the MgO(100) surface slab, vibrational modes at Γ, X, M high symmetric points are included in the spectrum in Fig. 4(b). The few existing experimental measurements [53, 54] (solid circles in Fig. 4b) suggest our phonon calculations for MgO(100) surfaces give reasonable results. Based on our phonon calculations, the Helmholtz free energies as a function of temperature for bulk MgO and for the MgO(100) slab were calculated using Eqs.(1)-(5); the results are shown in Fig. 5. It can be seen that the free energies of bulk MgO bulk (dotted line) and the MgO(100) slab (dashed line) decrease with increasing temperature. The resultant surface free energy for MgO(100) (solid line) deceases from 0.86 J/m^2 to 0.52 J/m^2 as the temperature varies from 0 K to 800 K. In Fig. 5, the slope of the surface energy is the negative of the surface entropy ($S_{surface} = -\frac{\partial \gamma}{\partial T}$). This follows from the Gibbs-Duheim equation. Details of this derivation can be found in [55].

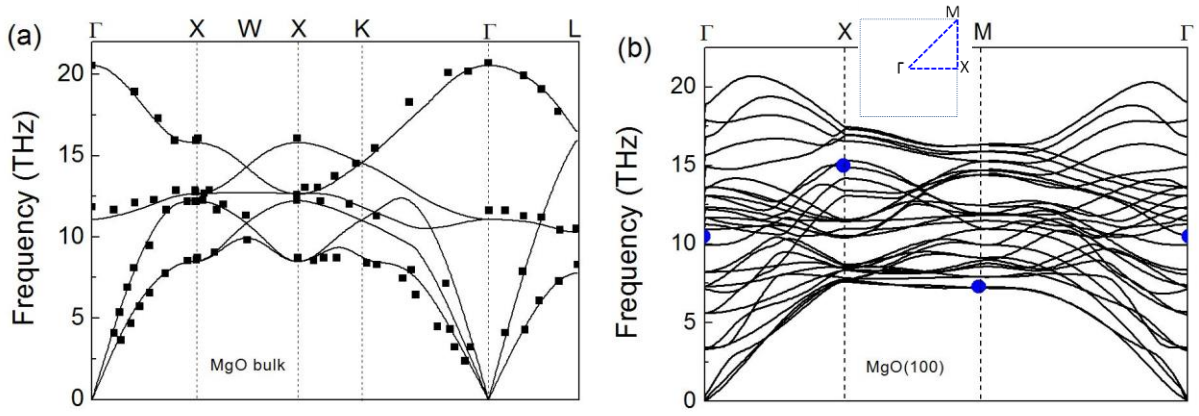

Fig. 4. Phonon spectra of (a) MgO bulk; (b) MgO(100) slab (inset represents the 2D first Brillouin Zone indexed with high symmetric points). Solid lines are present calculations; solid squares and circles are experimental measurements [52-54].

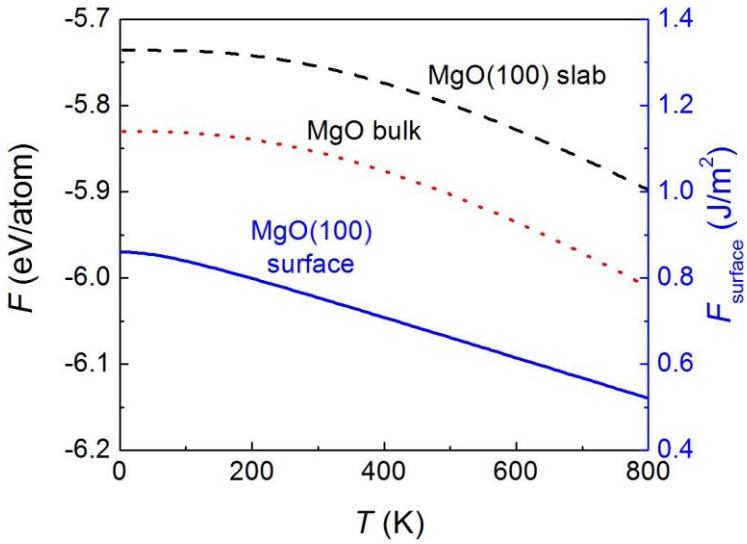

Fig. 5. Helmholtz free energy as a function of temperature of MgO bulk (dashed line), MgO(100) slab (dotted line) and MgO(100) surface (solid line).

The phonon spectra of Mg bulk and a Mg(0001) slab including several high symmetry points (Γ, K, M, A for bulk, Γ, K, M for the surface slab) are shown (solid lines) in Fig. 6(a) and (b), respectively, together with experimental data [56]. Good agreement between the calculated and experimental values is observed. Fig. 7 shows the Helmholtz free energy as a function of temperature (<800 K) for bulk Mg, the Mg (0001) slab and the Mg(0001) surface, all of which decrease with increasing temperature. The surface free energy of Mg(0001)

decreases from 0.520 J/m^2 to 0.486 J/m^2 when the temperature increases up to 800K. Again, the slope is the negative of the surface entropy.

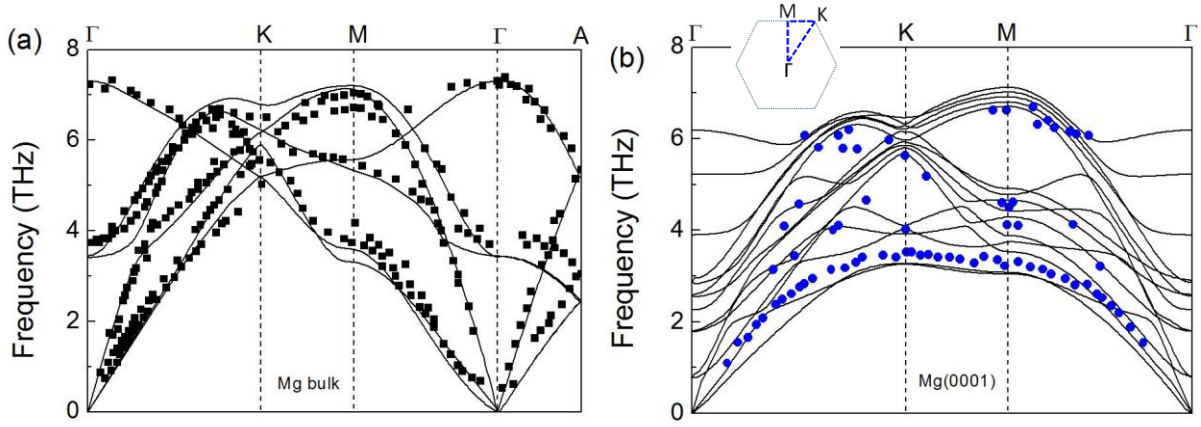

Fig. 6. Phonon spectra of (a) Mg bulk; (b) Mg(0001) (inset represents the 2D first Brillouin Zone indexed with high symmetric points) slab: solid lines – present calculations; solid squares and circles – experimental measurements [56].

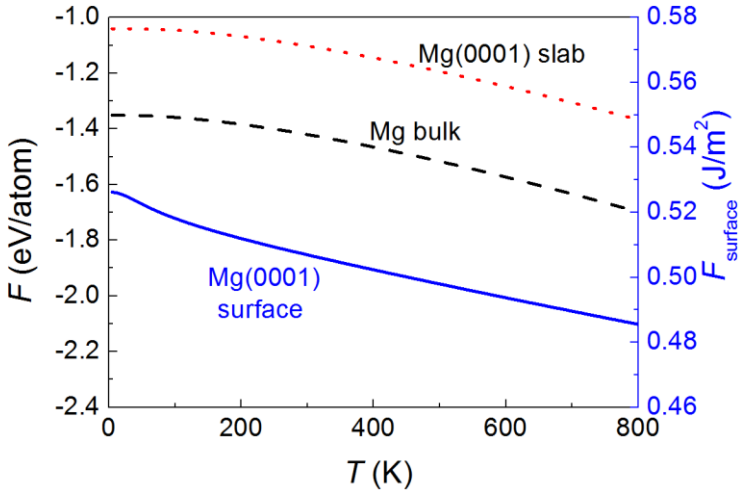

Fig. 7. Helmholtz free energy as a function of temperature of Mg bulk (dash line), Mg (0001) slab (dotted line) and Mg(0001) surface (solid line).

As has been shown above, good agreement between experiments and current phonon calculations for bulk phases and surface slabs are reached. In the following, we perform phonon calculations for the two interface models and calculate their temperature dependent

interfacial free energies according to Eq. (5). First of all, the phonon spectra (including four high symmetry points) of the two interface models with Mg-Mg and Mg-O stacking at the interface planes are shown in Fig. 8(a) and (b), respectively. Based on the phonon spectra in Fig. 8(a), the vibrational free energy of the interface slab (the term $F^{AB}_{slab_{vib}}$ in Eq. 5) with Mg-Mg stacking sequence is obtained, as shown by the open-square symbol-line in Fig. 9. In addition, we performed phonon calculations and calculated the vibrational free energies (open-circle & open-triangle symbol-lines in Fig. 9) for the two strained supercells of the component phases (the term Fs_{vib} in Eq. 5) of this interface model (Mg-Mg stacking). Finally, the interfacial free energy (according to Eq. 5) as a function of temperature for the Mg(0001)/MgO(100) interface with Mg-Mg stacking at the interface planes is obtained, as shown by the filled-square symbol-line in Fig. 10(a). Similar calculations have been done for the interface model with Mg-O stacking at the interface plane. Its vibrational free energies of the interface slab and the two strained supercells are shown by the solids lines in Fig. 9, from which the interfacial free energy for the Mg(0001)/MgO(100) interface with Mg-O stacking at the interface planes is calculated as a function of temperature (thick solid line in Fig. 10a).

We also investigated the vibrational strain energy of each component in the interface models according to the second term in Eq. (6). Fig. 10(b) gives the vibrational strain contributions of component phases in the two interface models. The vibrational strain energies are dependent on temperature and increase linearly with the increase of temperature. However, we notice that the magnitude of these values is very small, up to ~0.02 eV and ~0.03 eV per unit interface for the MgO(100) and Mg(0001) component, respectively, when the temperature is increased to 800 K.

The influences of the vibrational strain energies to interfacial free energy are demonstrated in Fig. 10(a). The filled-triangle symbol-line and the thin solid line represent the interfacial free energies excluding the vibrational strain contribution of the

Mg(0001)/MgO(100) interface with Mg-Mg and Mg-O stacking at the interface planes, respectively. These are computed using Eq. (7) by neglecting the term $Es_{vib}(T)$. The difference of interfacial free energy between cases of with and without the vibrational strain contribution is no more than ~0.02-0.03 J/m^2 when the temperature is increased to 800 K. This is very much reaching the limit of the current calculation accuracy, i.e., ~0.01 J/m^2. Therefore, we think that, at low temperatures (e.g., <~800 K), it makes sense to neglect the vibrational strain contribution to the interfacial free energy when a very high accuracy of simulation is not necessary. In this case the second term in Eq. (6) can be omitted. Eq. (6) can then be replaced by $E_s(T) = E_s(0\text{K}) = U^0_S - NU^0_{bulk}$. Consequently, interfacial free energies as a function temperature can be approximately calculated using Eq. (7) by eliminating the term $Es_{vib}(T)$. However, this term $Es_{vib}(T)$ may be crucial at high temperatures close to the melting point (e.g., >800 K for Mg bulk). The strain could also play a complicated role in frequency shifting (positively or negatively) of different modes (LO, LA, TO, TA) in the phonon dispersions for different systems [57]. It has also been suggested that the compressive (tensile) strain decreases (increases) the specific heat capacity at constant pressure (i.e., C_V) and the C_V trend with strain is controlled by the high energy phonon dispersion [58].

According to first-principles calculation results shown in Fig. 10(a), the interfacial free energies decrease with increasing temperature. The temperature dependence of interfacial free energies (according to Eq. 5) of the Mg(0001)/MgO(100) interface, $\gamma(T)$ (unit: J/m^2), can be well described with the following piecewise function:

For Mg-Mg stacking:

$$\gamma(T) = \begin{cases} 1.048 - 3.534\times10^{-5}T - 3.231\times10^{-7}T^2 & (0\text{ K} < T < 300\text{ K}) \\ 1.095 - 2.797\times10^{-4}T & (300\text{ K} < T < 800\text{ K}) \end{cases} \quad (11)$$

For Mg-O stacking:

$$\gamma(T) = 0.910 - 2.546\times10^{-5}T - 3.232\times10^{-7}T^2 \quad (0\text{ K} < T < 300\text{ K})$$

$$0.957 - 2.700\times10^{-4}T \qquad (300\ \mathrm{K} < T < 800\ \mathrm{K}) \qquad (12)$$

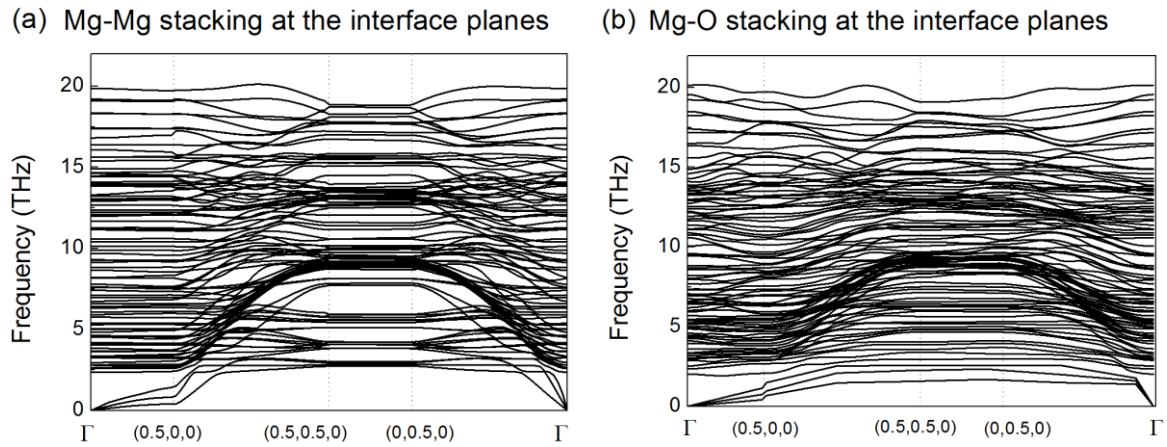

Fig. 8. Phonon spectra of Mg(0001)/MgO(100) interface models with (a) Mg-Mg and (b) Mg-O stacking sequences at the interface planes.

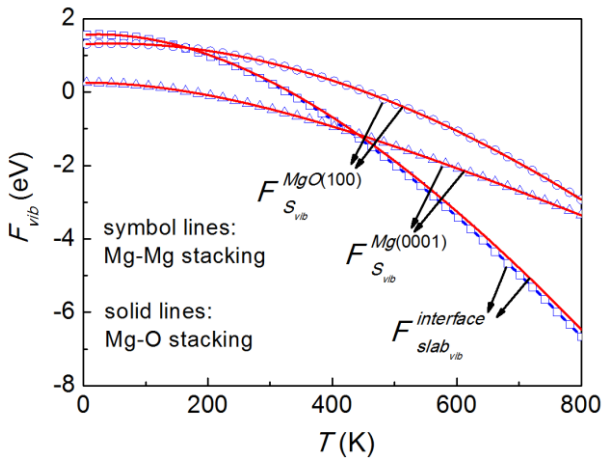

Fig. 9. Vibrational free energies of an interface slab and the two strained supercells of component phases in the ($\sqrt{3}\times1$)/(2×1) Mg(0001)/MgO(100) interfaces (Mg-Mg and Mg-O stacking at the interface planes) consisting of 5 atomic layers of each component.

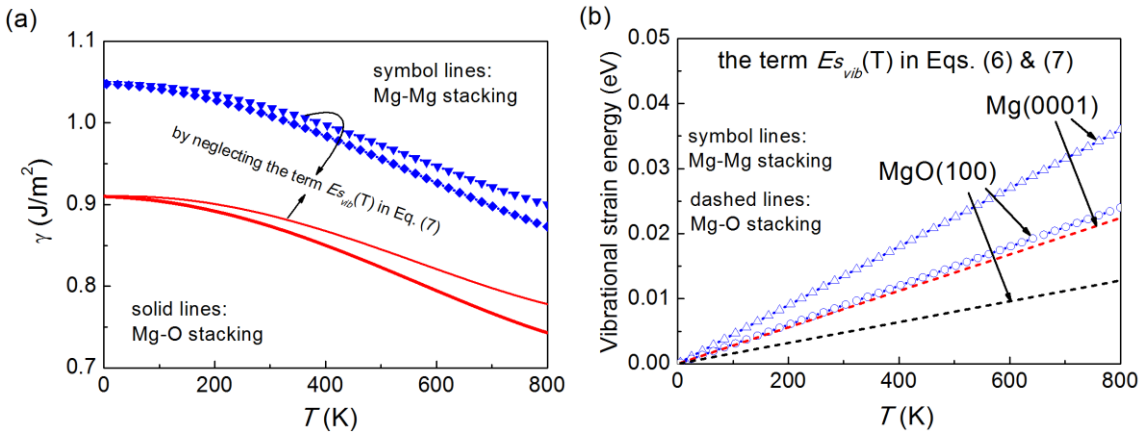

Fig. 10. (a) interfacial free energies as a function of temperature and (b) the corresponding vibrational strain energies (the term $Es_{vib}(T)$ in Eqs. 6 & 7) of each component of the two Mg(0001)/MgO(100) interfaces with Mg-Mg and Mg-O stacking sequences at the interface planes.

To summarize, the temperature dependence of the interfacial free energy of the Mg(0001)/MgO(100) interface was calculated using first-principles calculations. In principle, the temperature dependencies of interfacial free energies for various crystal orientations of Mg/MgO interfaces and different solid interfaces can be obtained using this method (Section II). This is applicable to a wide range of problems involving solid state interfacial thermodynamics and kinetics. In the following, we show how our first-principles calculations can be applied to model the interfacial free energy as a function of both temperature and particle size in an MgO NPs reinforced Mg matrix nanocomposite material.

5. Free energy and strengthening of metal matrix nanocomposites

By adding up to 1.0 vol% of nanosize MgO particles into Mg, Goh et al. [59] have obtained improved microhardness, yield and tensile strengths, and modulus in the composites relative to pure metal Mg. It is generally considered that the enhanced mechanical properties (e.g. microhardness) of nanocomposites can be mainly attributed to the pinning effect of nanosized

particles which hinder the movement of dislocations in the matrix. However, reducing the sizes of NPs results in higher interfacial tension (or interfacial energy) between melts of matrices and the solid NPs [60], and hence higher energies for the NPs in the melts to be dispersed. Reducing the interfacial energies also stabilises the solid particles, reducing the rate at which coarsening occurs. Though molecular dynamics simulations to calculate the interfacial free energy of the solid-liquid Mg/MgO interfaces are not available due to the lack of potentials to describe the interatomic interactions at the interfaces, our DFT calculations on solid state Mg/MgO interfaces in the nanocomposites may be able to provide useful insights into the stability of the particles in the solid matrix.

The total free energy of a metal matrix nanocomposite, $F_{tot}(T,D)$, as a function of temperature T and NP size D, including the contribution from the heterophase interfaces between matrix and embedded particles is given by:

$$F_{tot}(T,D) = N_m F_m(T) + N_p F_p(T) + \gamma(T) S_{tot}(D) \quad (13)$$

where N_m and N_p are the number of atoms in the matrix and NPs, respectively. F_m and F_p are the free energies per atom in the regions of matrix and NPs, respectively, and γ is the interfacial free energy. The product γS_{tot} is the excess (interfacial) free energy (F_{exc}) of the nanocomposite relative to the corresponding bulk systems. If the NPs are spherical then the total area of the heterophase interfaces is $S_{tot}(D) = \pi \sum_n D_n^2$, where D_n is the diameter of the n^{th} NP. Using Eq. (13) we can obtain the free energy for a composite system of metal Mg reinforced by MgO NPs using the results of our first-principles calculations presented in Figs. 5, 7 & 10(a).

We consider when 0.5 and 1.0 vol% MgO NPs are added to solid metal Mg, and obtain the excess free energies as a function of temperature and NP size as shown in Fig. 11(a) and (b), respectively. It is seen that the excess free energy increases with a decrease of particle size at fixed temperature; this is a consequence of the increase in both the number of particles

and the surface area to volume ratio as the particle size decreases (see Fig. 11c). The excess free energy in the nanocomposites is increased ~10 times when the particle size is reduced from 100 nm to 10 nm. For example, the excess free energies of nanocomposites with additions of 0.5 and 1.0 vol% MgO NPs are increased from 4.3 to 42.8 J/mol and from 8.8 to 88.0 J/mol, respectively. This implies that, at a given concentration, nanocomposites with smaller NPs have a stronger tendency to reduce the energy of the system by coarsening or coalescing to reduce the total interfacial area. As a result, the mechanical properties of the nanocomposite materials may degrade.

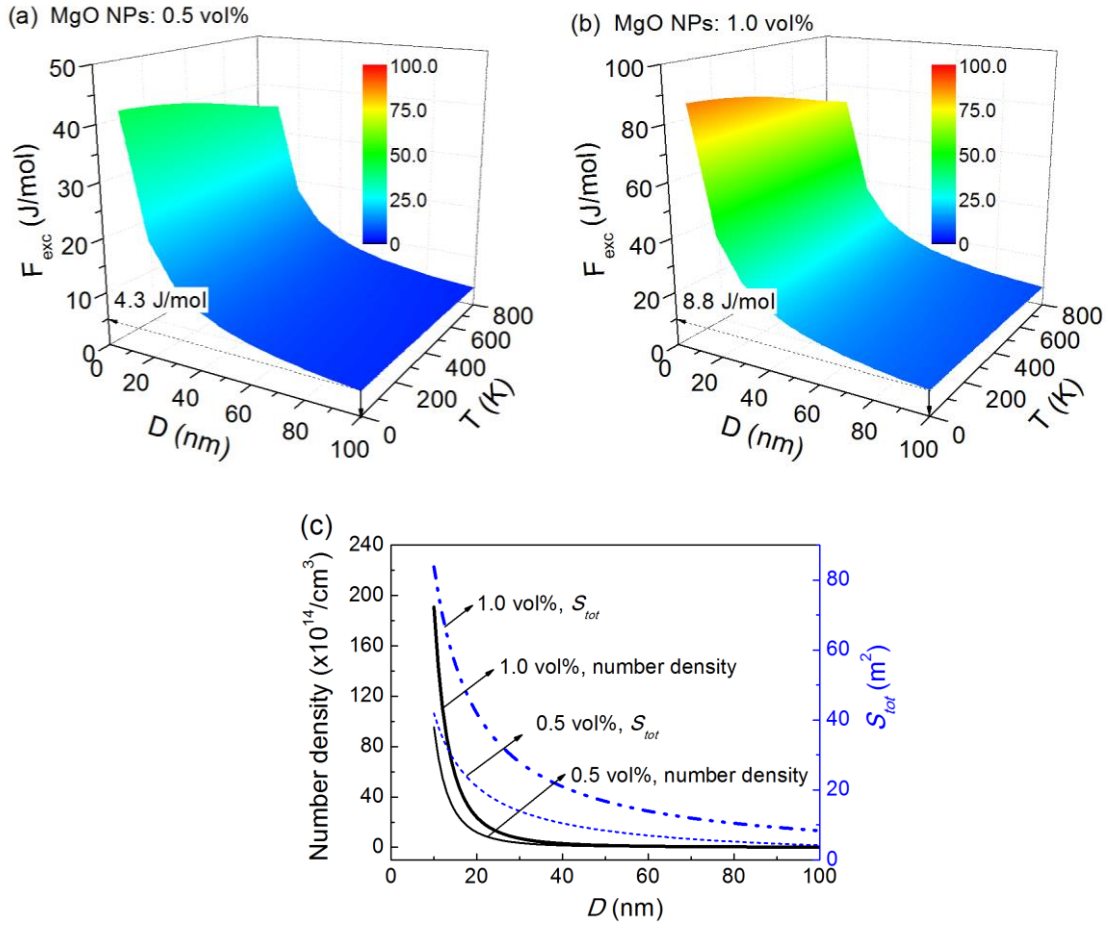

Fig. 11. (Colour online) Excess free energy F_{exc} as a function of temperature and particles size: (a) 0.5 vol % MgO, (b) 1.0 vol % MgO; (c) number density of NPs and total area of heterophase interfaces as a function of particle size for the system of metal Mg reinforced by MgO NPs.

Nanoparticle composites strengthen the matrix by impeding the movement of dislocations [62]. For NPs that are small relative to the spacing between them, dislocations are likely to cut through the NP, and the strengthening is then described by Eq. (14) [62],

$$\tau = \frac{\pi D\gamma}{2Lb} \tag{14}$$

where τ is the strength of nanocomposites, D is the MgO NP size, γ is the NP/matrix interfacial free energy, L is the distance between NPs, and b is the Burgers vector of dislocations. The degree of strengthening thus depends strongly on the NP size, as well as the NP/matrix interfacial free energy. With an increase of NP size, cutting through becomes more and more difficult, and dislocations are thus more likely to bow around the NPs at large enough size. This leads to Orowan strengthening [63], which can be described by Eq. (15) [62].

$$\tau = \frac{Gb}{L-D} \tag{15}$$

where G is the shear modulus of Mg. If we take note of the linear relationship between particle size (D) and separation (L) at fixed concentration, then we find from Eq. (15) that for dislocation bowing the strength is inversely proportional to the NP size. Therefore, there exists a concentration dependent critical NP size (D_c) at which the strengthening is a maximum: this is obtained when Eq. (14) and (15) are equal. The larger the interfacial energy and the larger the concentration of nanoparticles, the smaller the particles need to be. So we have a tension between wanting large particles to reduce their surface area, and thus making them more stable, and not allowing the particles to become too large so that they provide sufficient strengthening. If we can reduce the interfacial energy, then we can allow for larger particles without reducing the strengthening, while also improving stability.

It should be noted that Eqs. (14) and (15) are only valid when neighbouring NPs in the matrix are well separated so that there is no significant interaction between them. This is only true when the NP concentration is relatively low, e.g. << 1.0 vol%. In addition, a number of

simplifying assumptions have been made in the above model. (I) We considered only the heterophase interfaces between NPs and matrix, as the free energy contribution from grain boundaries within the metal matrix is negligible when the grain size is in excess of the nanometer scale. (II) The atomic structure at the interface is invariant as the particle size is reduced to the nanoscale, as well as when there is a change of temperature in the system. However, the interface thickness may increase when the particle size and/or the grain size in the matrix are below a few nanometers [61]. Our calculations thus only apply to systems with NPs of size greater than 10 nm embedded in matrices with a negligible grain boundary component (i.e., grain size of matrix >> 100 nm). (III) Only the Mg(0001)/MgO(100) interfacial orientation is considered. It has been reported that the other crystal orientations of Mg/MgO interfaces possess much higher interfacial energies in the ground state, e.g., 1.40~1.71 J/m^2 of Mg(0001)/MgO(110) and 4.30~4.92 J/m^2 of Mg(0001)/MgO(111) [41]. Therefore, the interfacial free energy in Fig. 10 is actually the lower bound for the Mg/MgO MMNC as the consideration of other crystal orientations of Mg/MgO interfaces will increase the interfacial energy of the Mg/MgO MMNC.

6. Conclusions

In this paper, we used DFT to compute bulk, surface and interfacial Helmholtz free energies as a function of temperature for a heterophase system found in solid nanomaterials formed from Mg and MgO. When temperature increases from 0 K to 800 K, the Helmholtz free energies of Mg(0001), MgO(100) surfaces decrease from 0.520 J/m^2 to 0.486 J/m^2, from 0.86 J/m^2 to 0.52 J/m^2, respectively, and the Mg(0001)/MgO(100) interfaces with Mg-Mg and Mg-O stacking sequences at the interface planes are reduced from 1.048 J/m^2 to 0.873 J/m^2 and 0.910 to 0.743 J/m^2, respectively. These results were used to analyse the interfacial free energy of MgO nanoparticles within an Mg metal matrix nanocomposite as a function of temperature and nanoparticle size. It was found that interfacial free energy increases with the

decrease of particle size at a constant temperature and the excess free energy in the nanocomposites is increased ~10 times when the particle size is reduced from 100 nm to 10 nm.

Acknowledgements

The authors wish to acknowledge financial support from the ExoMet Project (which is co-funded by the European Commission in the 7th Framework Programme (contract FP7-NMP3-LA-2012-280421), by the European Space Agency and by the individual partner organisations), the EPSRC (EP/I02249X/1) and the Research Complex at Harwell. This work made use of the facilities of N8 HPC provided and funded by the N8 consortium and EPSRC (Grant No.EP/K000225/1) and the Imperial College London High Performance Computing service.

References

[1] Q. Jiang, H.M. Lu, Surf. Sci. Rep., 63 (2008) 427-464.

[2] D. Myers, Surfaces, Interfaces, and Colloids : Principles and Applications, John Wiley & Sons, Inc, New York, 1999.

[3] Y. Feng, B. Wu, H.K. Yuan, H. Chen, J. Alloys Compd., 623 (2015) 29-35.

[4] A. Mortensen, J. Llorca, Annu. Rev. Mater. Res., 40 (2010) 243-270.

[5] J. Hirsch, T. Al-Samman, Acta Mater., 61 (2013) 818-843.

[6] S.I. Cha, K.T. Kim, S.N. Arshad, C.B. Mo, S.H. Hong, Adv. Mater., 17 (2005) 1377-1381.

[7] S.C. Tjong, Mater. Sci. Eng., R, 74 (2013) 281-350.

[8] Z. Sadeghian, B. Lotfi, M.H. Enayati, P. Beiss, J. Alloys Compd., 509 (2011) 7758-7763.

[9] H.P. Liu, S.Y. Zhou, X.C. Li, J. Manuf. Sci. E-T. ASME, 135 (2013) 011013.

[10] S. Chatterjee, A.B. Mallick, Mater. Sci. Forum, 736 (2013) 72-80.

[11] M. Paramsothy, X.H. Tan, J. Chan, R. Kwok, M. Gupta, J. Alloys Compd., 545 (2012) 12-18.

[12] J. Hutter, M. Iannuzzi, F. Schiffmann, J. VandeVondele, Wires. Comput. Mol. Sci., 4 (2014) 15-25.

[13] L. Martin, G. Vallverdu, H. Martinez, F. Le Cras, I. Baraille, J. Mater. Chem., 22 (2012) 22063-22071.

[14] K. Li, Z.G. Sun, F. Wang, N.G. Zhou, X.W. Hu, Appl. Surf. Sci., 270 (2013) 584-589.

[15] M. Asta, J.J. Hoyt, A. Karma, Phys. Rev. B, 66 (2002) 100101.

[16] S. Angioletti-Uberti, M. Ceriotti, P.D. Lee, M.W. Finnis, Phys. Rev. B, 81 (2010) 125416.

[17] J.J. Eggleston, G.B. McFadden, P.W. Voorhees, Phys. D, 150 (2001) 91-103.

[18] I. Steinbach, Modell. Simul. Mater. Sci. Eng., 17 (2009) 073001.

[19] X.J. Hu, Y.G. Shen, Appl. Phys. Lett., 94 (2009) 093111.

[20] K. Binder, B. Block, S.K. Das, P. Virnau, D. Winter, J. Stat. Phys., 144 (2011) 690-729.

[21] J.S. Wang, A. Horsfield, U. Schwingenschlogl, P.D. Lee, Phys. Rev. B, 82 (2010) 184203.

[22] J.S. Wang, A. Horsfield, P.D. Lee, P. Brommer, Phys. Rev. B, 82 (2010) 144203.

[23] N.S. Sidorov, A.V. Palnichenko, O.M. Vyaselev, Phys. C, 480 (2012) 123-125.

[24] N.S. Sidorov, A.V. Palnichenko, D.V. Shakhrai, V.V. Avdonin, O.M. Vyaselev, S.S. Khasanov, Phys. C, 488 (2013) 18-24.

[25] K. Jimbo, S. Nakagawa, Highly (100) oriented MgO growth on thin Mg layer in MTJ structure, in: The 2nd International Symposium on Advanced Magnetic Materials and Applications, Sendai, Japan, 2011, pp. 012118.

[26] H. Yang, S.H. Yang, S. Parkin, AIP Adv., 2 (2012).

[27] Y. Wang, Z. Fan, X. Zhou, G.E. Thompson, Philos. Mag. Lett., 91 (2011) 516-529.

[28] Y. Ortega, D.F. Hevia, J. Oviedo, M.A. San-Miguel, Appl. Surf. Sci., 294 (2014) 42-48.

[29] K. Parlinski, Phys. Rev. B, 74 (2006) 184309.

[30] D. Matsunaka, Y. Shibutani, Phys. Rev. B, 77 (2008) 165435.

[31] W. Pfeiler, Alloy Physics : A Comprehensive Reference, Wiley-VCH, Weinheim, 2007.

[32] Y. Mishima, S. Ochiai, T. Suzuki, Acta Metall., 33 (1985) 1161-1169.

[33] W.W. Xu, X.Y. Song, Z.X. Zhang, Appl. Phys. Lett., 97 (2010) 181911.

[34] S. Baroni, S. de Gironcoli, A. Dal Corso, P. Giannozzi, Rev. Mod. Phys., 73 (2001) 515-562.

[35] C. Kittel, P. McEuen, Introduction to Solid State Physics, John Wiley & Sons, Inc, New York ; Chichester, 2005.

[36] X.G. Lu, M. Selleby, B. Sundman, Acta Mater., 55 (2007) 1215-1226.

[37] M.W. Finnis, J. Phys. D: Condens. Matter, 8 (1996) 5811-5836.

[38] B.E. Hayden, E. Schweizer, R. Kotz, A.M. Bradshaw, Surf. Sci., 111 (1981) 26-38.

[39] B.J. Kooi, G. Palasantzas, J.T.M. De Hosson, Appl. Phys. Lett., 89 (2006) 161914.

[40] See Supplemental Material at [URL will be inserted by publisher] for a discussion of the relative energetics of different orientation relations between Mg and MgO at an Mg/MgO interface.

[41] E.T. Dong, P. Shen, L.X. Shi, D. Zhang, Q.C. Jiang, J. Mater. Sci., 48 (2013) 6008-6017.

[42] N.W. Ashcroft, N.D. Mermin, Solid State Physics, Holt, Rinehart and Winston, New York, 1976.

[43] J. Goniakowski, C. Noguera, Phys. Rev. B, 60 (1999) 16120-16128.

[44] E. Wachowicz, A. Kiejna, J. Phys. D: Condens. Matter, 13 (2001) 10767-10776.

[45] S.J. Clark, M.D. Segall, C.J. Pickard, P.J. Hasnip, M.J. Probert, K. Refson, M.C. Payne, Zeitschrift Fur Kristallographie, 220 (2005) 567-570.

[46] J.P. Perdew, K. Burke, M. Ernzerhof, Phys. Rev. Lett., 77 (1996) 3865-3868.

[47] H.J. Monkhorst, J.D. Pack, Phys. Rev. B, 13 (1976) 5188-5192.

[48] B.G. Pfrommer, M. Cote, S.G. Louie, M.L. Cohen, J. Comput. Phys., 131 (1997) 233-240.

[49] Z.G. Mao, C. Booth-Morrison, E. Plotnikov, D.N. Seidman, J. Mater. Sci., 47 (2012) 7653-7659.

[50] A.R. Westwood, D.L. Goldheim, J. Appl. Phys., 34 (1963) 3335-3339.

[51] P. Broqvist, H. Gronbeck, I. Panas, Surf. Sci., 554 (2004) 262-271.

[52] M.J. Sangster, G. Peckham, Saunders.Dh, J. Phys. C, 3 (1970) 1026-1036.

[53] K.H. Rieder, E.M. Horl, Phys. Rev. Lett., 20 (1968) 209-211.

[54] K.H. Rieder, Surf. Sci., 26 (1971) 637-648.

[55] G.H. Meier, Thermodynamics of surfaces and interfaces : concepts in inorganic materials, Cambridge University Press, Cambridge, 2014.

[56] Ismail, P. Hofmann, E.W. Plummer, C. Bungaro, W. Kress, Phys. Rev. B, 62 (2000) 17012-17019.

[57] Z. Sui, I.P. Herman, Phys. Rev. B, 48 (1993) 17938-17953.

[58] A. Paul, G. Klimeck, Appl. Phys. Lett., 99 (2011) 083115.

[59] C.S. Goh, M. Gupta, J. Wei, L.C. Lee, J. Compos. Mater., 41 (2007) 2325-2335.

[60] V. Khoshkava, M.R. Kamal, Biomacromolecules, 14 (2013) 3155-3163.

[61] W.W. Xu, X.Y. Song, N.D. Lu, C. Huang, Acta Mater., 58 (2010) 396-407.

[62] W.D. Callister, D.G. Rethwisch, Fundamentals of Materials Science and Engineering: an Integrated Approach, 4th ed., John Wiley and Sons, Hoboken, N.J., 2012.

[63] E. Orowan, Symposium on Internal Stresses in Metals and Alloys, Institute of Metals, London, 1948.

Captions:

Fig. 1. Two approaches for constructing the interface model using slab techniques: (a) alternating slabs of A and B cleaved from bulk phases along certain crystallographic orientations; (b) surface/interface units are separated from their periodic images by vacuum. Surface and interface cell units repeat in the directions normal to the surface/interface planes.

Fig. 2. Computing interfacial free energy based on DFT: (a) by subtracting off total energies of relaxed A and B from that of the relaxed interface unit, the result includes interfacial free energy (γ) and the strain energy (E_s); (b) by subtracting off total energies of strained A and B from that of relaxed interface unit, the result includes only the interfacial free energy (γ).

Fig. 3. (Colour online) Atomic structures of computational cells used for the DFT calculations: (I) Mg(0001) surface; (II) MgO(100) surface; (III) $Mg(0001)_{hcp}/MgO(100)_{fcc}$ interface (Mg-Mg stacking at the interface planes) viewed along an interface plane; and (IV) the corresponding top-views. *a*, *b* and *c* are the lattice parameters and the arrows show crystal orientations.

Fig. 4. Phonon spectra of (a) MgO bulk; (b) MgO(100) slab (inset represents the 2D first Brillouin Zone indexed with high symmetric points). Solid lines are present calculations; solid squares and circles are experimental measurements [52-54].

Fig. 5. Helmholtz free energy as a function of temperature of MgO bulk (dashed line), MgO(100) slab (dotted line) and MgO(100) surface (solid line).

Fig. 6. Phonon spectra of (a) Mg bulk; (b) Mg(0001) (inset represents the 2D first Brillouin Zone indexed with high symmetric points) slab: solid lines – present calculations; solid squares and circles – experimental measurements [56].

Fig. 7. Helmholtz free energy as a function of temperature of Mg bulk (dash line), Mg (0001) slab (dotted line) and Mg(0001) surface (solid line).

Fig. 8. Phonon spectra of Mg(0001)/MgO(100) interface models with (a) Mg-Mg and (b) Mg-O stacking sequences at the interface planes.

Fig. 9. Vibrational free energies of an interface slab and the two strained supercells of component phases in the $(\sqrt{3}\times1)/(2\times1)$ Mg(0001)/MgO(100) interfaces (Mg-Mg and Mg-O stacking at the interface planes) consisting of 5 atomic layers of each component.

Fig. 10. (a) interfacial free energies as a function of temperature and (b) the corresponding vibrational strain energies (the term $ES_{vib}(T)$ in Eqs. 6 & 7) of each component of the two Mg(0001)/MgO(100) interfaces with Mg-Mg and Mg-O stacking sequences at the interface planes.

Fig. 11. (Colour online) Excess free energy F_{exc} as a function of temperature and particles size: (a) 0.5 vol % MgO, (b) 1.0 vol % MgO; (c) Number density of nanoparticles and total area of heterophase interfaces as a function of particle size for the system of metal Mg reinforced by MgO nanoparticles.